Renewable Energy 212 (2023) 478–491

Contents lists available at ScienceDirect

Renewable Energy

journal homepage: www.elsevier.com/locate/renene

Implications of spring-like air compressibility effects in floating coaxial-duct OWCs: Experimental and numerical investigation

J.C.C. Portillo *, L.M.C. Gato, J.C.C. Henriques, A.F.O. Falcão

IDMEC, Instituto Superior Técnico, Universidade de Lisboa, Av. Rovisco Pais 1, 1049-001 Lisbon, Portugal

ARTICLE INFO

Keywords:
Wave energy
Floating oscillating water column
Coaxial-duct
Compressibility effects
Equicompressum critical points
Modelica

ABSTRACT

The paper analyses the spring-like air compressibility effect in coaxial-duct oscillating-water-column (CD-OWC) wave energy converters (WECs). This is accomplished through a novel non-linear time-domain model for OWC WECs implemented in the object-oriented language Modelica. Good agreement was observed between numerical and physical model testing results. The air chamber volume significantly affected the spring-like air compressibility effect and the converter performance. Another significant factor is the damping level of the power take-off system. Both fixed and floating CD-OWC versions were numerically investigated, focusing on the compressibility effect. Differences were found mainly due to the additional degrees of freedom in floating configurations. In general, numerical and experimental results showed that air compressibility might positively or negatively affect device power performance in regular waves, depending on whether the frequency is within or out of an interval defined by critical frequencies. Some particular points were observed and categorised as Equicompressum Nullum and Equicompressum critical points, representing different characteristics. Knowledge of these critical values might be important in OWC control. Finally, some applications of the CD-OWC concept are discussed, including considerations on the power output level provided by biradial and Wells air turbines.

1. Introduction

The energy sustainability of our societies requires research, development, and innovation actions on renewable energy sources and, among them, sea wave energy. Public policies and instruments are being directed to support these actions sustainably [1–4]. In Europe, it has been recognised that a sustainable ocean energy mix could generate a quarter of the EU's electricity needs by 2050. The energy mix shall involve offshore wind, wave and tidal energy [5].

The sea waves are known to be a vast renewable energy resource [6,7] whose utilisation requires the development of efficient technologies in balance with the environment. Scientific and technological knowledge associated with wave energy conversion has been boosted in the last few years [8–11]. Unlike the horizontal axis wind turbine, there is still no clear winning concept for wave energy conversion [12,13]. An initiative that should be mentioned is the EuropeWave, an innovative R&D programme for competitive pre-commercial procurement of wave energy technologies [13]. Comprehensive development processes have already been proposed for wave energy conversion technologies [14–16].

The oscillating-water-column (OWC) type of wave energy converter (WEC) is widely regarded as the simplest, most reliable, and extensively studied type of wave energy converter [9,17–20]. Generally, it consists of a partly submerged hollow structure, with an opening below water level, that can be fixed (e.g. bottom standing or integrated into breakwaters) or floating (which may include wave energy platforms, hybrid power floating systems or other multi-purpose platforms). The air trapped above the inner free surface is alternately compressed and decompressed by wave action and, in most cases, is forced to flow in reciprocating motion through a self-rectifying air turbine that connects the OWC air chamber to the atmosphere [19]. The rotational direction in these turbines remains unchanged regardless of the airflow direction. The axial-flow Wells turbine is the most popular self-rectifying air turbine since it was patented in 1976 [21,22]. However, other types of self-rectifying air turbines, of axial- and radial-flow types, have also been proposed, developed, and used [19,23].

If the efficiency of wave energy absorption is a prime requirement, the structure must be relatively large. Its size and shape should be optimised depending on the local wave climate. To avoid green water from being ingested by the air turbine in rough seas, the air chamber volume divided by the inner free-surface area typically ranges between 3 and 8 m [24]. It should be noted that the air chamber volume should be large enough to ensure turbine safety. Indeed, as the air volume

* Corresponding author.
E-mail addresses: juan.portillo@tecnico.ulisboa.pt (J.C.C. Portillo), luis.gato@tecnico.ulisboa.pt (L.M.C. Gato), joaochenriques@tecnico.ulisboa.pt (J.C.C. Henriques), antonio.falcao@tecnico.ulisboa.pt (A.F.O. Falcão).

https://doi.org/10.1016/j.renene.2023.04.143
Received 8 November 2022; Received in revised form 22 April 2023; Accepted 29 April 2023
Available online 4 May 2023

increases to very large values, the amplitude of the inner air pressure oscillation becomes very small, and so does the capacity to absorb energy from the waves [25].

The spring-like air compressibility effect in the air chamber may significantly affect the efficiency of full-sized OWCs. It has been studied theoretically for the first time in Ref. [26], and many times after that; for a review, see Ref. [27]. Depending on converter geometry, power take-off system characteristics, and incident wave conditions, this effect may be beneficial or detrimental to wave energy absorption. It may be accounted for in model testing in a wave tank, but that has rarely been done [28].

Theoretical models have been presented accounting for air compressibility effects on OWC performance [29–34]. A sophisticated model in which the air compression/decompression process is allowed to be non-isentropic (due to aerodynamic losses in the turbine) is reported in Ref. [29]; it was found that the isentropic assumption in the air chamber provides a good approximation to the air compressibility effect on the time-averaged OWC performance. A recent theoretical investigation [28], with experimental validation, showed that, in regular waves, the air compressibility might affect positively or negatively the absorbed energy from the waves, depending on wave frequency and air chamber volume. In a given fixed-structure OWC converter subject to regular incident waves of frequency ω, it was shown that there is, in general, a frequency range $\omega_1 < \omega < \omega_2$ such that the air compressibility effect increases the amount of energy absorbed from the waves, the opposite being true if $\omega < \omega_1$ or $\omega > \omega_2$. The values of ω_1 and ω_2 depend on OWC geometry and are independent of (or weakly dependent on) turbine damping and wave amplitude. Other theoretical works like the one in Ref. [34] also reported that air compressibility might broaden the bandwidth of high extraction efficiency, i.e., positively influencing wave energy extraction.

Positive and negative compressibility effects upon OWC performance, mostly for fixed OWCs, have been reported in experimental and numerical studies in the published literature. In Ref. [35], it was found that neglecting compressibility effects may underpredict or overpredict power performance considerably by up to ±30% in terms of capture width ratio (CWR). Other studies reported only negative effects on the hydrodynamic performance, as in Refs. [32,36], with overestimations of up to about 10–12%. In Ref. [37], numerically obtained results showed over-predictions of up to 20% for a fixed-structure OWC equipped with Wells or impulse turbines. In another numerical work, Ref. [38], concerning a fixed-structure OWC, the increase in air chamber volume was found to decrease the peak CWR by up to 27%. Differently, in Ref. [39], for the analysed cases, it was found, both numerically (CFD) and experimentally, that effects associated with the compressibility of the air in the pneumatic chamber improved the OWC power performance. Maximum differences in CWR were found to be in the order of 30%. Nevertheless, these results should be interpreted with care because the scaling of the air chambers was relatively similar (about 1:3), and only Froude similitude was used (disregarding the different scaling required for the air chamber).

Another significant factor affecting OWCs' performance is the damping level of the power take-off system. Turbine damping has been extensively studied over the years. It depends on the type of turbine (e.g. Wells versus impulse), geometry, size, available pressure head to the turbine, and other operational conditions, such as rotational speed. Comprehensive studies of various case studies using different air turbines for fixed OWCs with consideration of compressibility effects in the air chamber can be found, for example, in Refs. [40,41]. In Ref. [40], a fixed OWC equipped with a Wells turbine was assessed using CFD and lump mass parameter approaches to study further the hysteretic behaviour reported firstly in Ref. [42]. Results demonstrated that the often discussed hysteresis was due to compressibility effects in the air chamber and not turbine aerodynamics. Complementary, Ref. [41] presents an in-depth analysis of Wells and biradial air turbines for the Mutriku wave power plant considering compressibility in the air chamber, highlighting the different overall behaviours and the significant effects of the different turbine types. Overall, as it is widely recognised, the optimisation of an OWC system must consider several parameters, among them the spring-like effect of air compressibility within the air chamber and the air turbine damping.

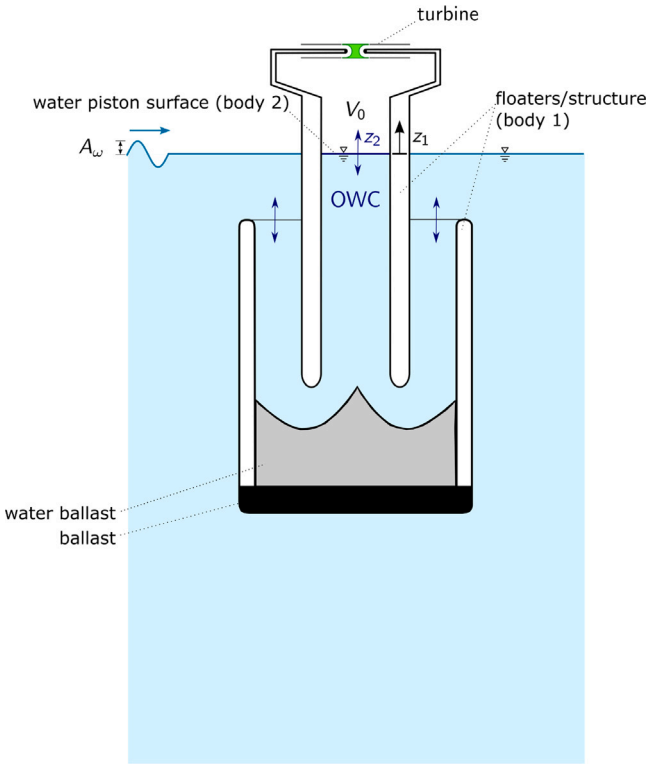

Fig. 1. Coaxial-duct OWC floating concept. Mooring lines are not represented.

The only experimental study of the air compressibility effect in a floating OWC equipped with orifices emulating self-rectifying air turbines appeared in Ref. [25]. It demonstrated the difficulties in incorporating the proper scaling for the air chamber volume and the effect on the motions of the floating system due to the need for an additional pneumatic tank, connection hoses, and other fittings. Regarding numerical modelling, a numerical CFD analysis was presented in Ref. [43] for a two-dimensional floating OWC considering only the heave degree of freedom; the effect of air compressibility upon the heave motion was found to be small.

The present paper investigates the effects of spring-like air compressibility in fixed and floating OWCs. Numerical models validated with experimental data were developed for the purpose. The system used for the investigation is the new floating OWC concept named coaxial-duct OWC wave energy converter (CD-OWC) [16,25,44,45]. The converter has a vertical axis of symmetry and consists of two coaxial cylindrical ducts interconnected at their bottom (see Fig. 1). The outer duct (totally submerged) is open to the sea at its top. The inner duct extends above sea level and communicates with the atmosphere through a self-rectifying air turbine mounted at its top. The device is characterised by the relatively small amplitude of its heaving oscillations that (unlike in the sparbuoy OWC) are found to play a minor role in the wave energy absorption process.

The paper is divided into the following sections. Section 2 presents the mathematical model used considering the compressibility of air in the pneumatic chamber and its implementation in the object-oriented and multiphysics language Modelica. Section 3 describes this work's floating CD-OWC wave energy converter. Section 4 presents the validation approach of the numerical model. Afterwards, numerical results with a focus on the spring-like compressibility effects are discussed in Section 5. This is followed by the conclusions in Section 6.

2. Time-domain model

This section introduces the theoretical modelling of the floating OWC converter considered in this work. The water flow field is assumed incompressible and irrotational. The wave amplitudes are assumed to be much smaller than the typical wavelengths, and the body-motion amplitudes are much smaller than the device's characteristic length, which allows linear water wave theory to be employed. The inner free surface of the OWC is modelled as a thin circular rigid piston whose density is equal to water density and whose diameter is much smaller than the wavelength.

Fig. 1 shows a cross-section of the two-body system. Body 1 is the physical floater, and body 2 is the thin rigid piston as in Ref. [46]. Sloshing modes are absent. A Cartesian coordinate system (x, y, z) is adopted, with the z-axis pointing vertically upwards and $z = 0$ at the free surface in the absence of waves.

The floater is allowed to oscillate with six degrees of freedom: surge (mode 1), sway (mode 2), heave (mode 3), roll (mode 4), pitch (mode 5), and yaw (mode 6). The thin piston is assumed to oscillate in heave (mode 9) while remaining horizontal. The vector $\mathbf{x}$ represents all modes for the two-body system, with time-dependent components x_i, where i is the mode index from $i = 1$ to 6 for the floater, and $i = 9$ for the piston. In the absence of waves, it is $x_i = 0$ for all values of i. The equations of motion may be found in Ref. [47] for an arbitrary number of oscillating bodies and in Ref. [48] for the specific case of two bodies oscillating in heave.

In the case of the two-body problem, the mass-inertia matrix $\mathbf{M}$ has 12×12 components. Regarding the thin piston, only the components associated with heave modes are considered, which correspond to the total mass (mass and added-mass) of the piston (component M_{99} in $\mathbf{M}$), and the coupling added-mass terms (M_{93} and M_{39}), assumed to exist only in the heave degrees of freedom (x_3 and x_9).

The time domain model considers air compressibility in the pneumatic chamber and rotational speed control of the air turbine. The model was implemented in the object-oriented language Modelica and validated through experimental data of a CD-OWC floating physical model at a scale of 1:40 [25].

2.1. OWC model: Equations of motion

The equations of motion for the ith mode in the time domain, can be written as

$$\sum_{j=1}^{6} \left((m_{ij} + A_{ij}^{\infty})\ddot{x}_j + R_{ij} + C_{ij}x_j \right) + \left(A_{39}^{\infty}\ddot{x}_9 + R_{39}\right) = F_{e,i} + F_{k,i} + F_{pto}\,, \quad i = 3\,, \tag{1}$$

$$\sum_{j=1}^{6} \left((m_{ij} + A_{ij}^{\infty})\ddot{x}_j + R_{ij} + C_{ij}x_j \right) = F_{e,i} + F_{k,i}\,, \quad i = 1,2,4,5,6\,, \tag{2}$$

$$(m_{99} + A_{99}^{\infty})\ddot{x}_9 + R_{99} + C_{99}x_9 + A_{93}^{\infty}\ddot{x}_3 + R_{93} = F_{e,p} - F_{pto}\,, \tag{3}$$

where x_j, $\dot{x}_j$, and $\ddot{x}_j$ are the displacement, velocity, and acceleration of the jth mode. $M_{ij} = m_{ij} + A_{ij}^{\infty}$ terms represent the components of the 12×12 total inertia matrix $\mathbf{M}$, i.e. each M_{ij} component includes the mass and the added mass contributions. Note that the inertia matrix $\mathbf{M}$ is symmetric and comprises many zero values. C_{ij} represents the components of the hydrostatic coefficients matrix $\mathbf{C}$. The terms $F_{k,i}$ are the forces associated with the mooring lines, which in this work were considered linear springs.

Furthermore, the excitation forces $F_{e,i}$ can be obtained as a sum of N components of frequency ω_n,

$$F_{e,i}(t) = \sum_{n=1}^{N} A_w(\omega_n)\,\Gamma_i(\omega_n)\,\cos\left(\omega_n t + \phi_1(\omega_n) + \phi_r(\omega_n)\right), \quad i = 1,2,\ldots,6\,, \tag{4}$$

where ω_n is the wave frequency of the regular wave component n, $\Gamma_i(\omega_n)$ represents the exciting force or moment response, and $A_w(\omega_n)$ is the incident wave amplitude, both as functions of regular wave component with frequency ω_n. $\phi_r(\omega_n)$ and $\phi_1(\omega_n)$ are the excitation response phase to the wave component and the phase in the wave generation (a uniform random phase), respectively.

The radiation terms R_{ij} represent the convolution integrals considered as functions of the radiation damping coefficients and given by

$$R_{ij} = \int_0^t \kappa_{ij}(t-\tau)\,\dot{x}_j(\tau)\mathrm{d}\tau\,, \tag{5}$$

where,

$$\kappa_{ij}(t) = \frac{2}{\pi}\int_0^{\infty} B_{ij}(\omega)\cos(\omega t)\mathrm{d}\omega\,, \tag{6}$$

represents the radiation impulse response functions. The convolution integral in Eq. (5) must be solved through direct integration or some other method. In this work, it was obtained using Prony's method formulation as presented in Ref. [41].

The coupling term $F_{pto,i}$ is connected to the relative heave motion of body 1 and body 2. This is why this term appears in equations of modes 3 and 9. The two-body coupling also requires the radiation cross-terms (A_{39}, A_{93}, R_{39} and R_{93}) to be considered.

The $F_{pto,i}$ term can be obtained from

$$F_{pto} = S_p\; p_{ac}(t)\,, \tag{7}$$

where S_p and $p_{ac}(t)$ represent the piston water plane area and the instantaneous pressure in the air chamber, respectively. Nevertheless, the knowledge of the pressure within the chamber to solve Eq. (7) requires solving simultaneously the complete system of equations, which includes the definition of the air chamber, turbine, generator, and control models. In the next sub-sections, these models are presented as used in this work. In addition, the model also considered additional viscous dissipation terms in the form of Morison-like equations for the drag component, calibrated based on experimental data.

2.2. Air chamber model

The air in the pneumatic chamber is assumed to satisfy the ideal gas equation

$$\rho_{ac} = \frac{p_{ac}}{R\,T_{ac}}, \tag{8}$$

where ρ_{ac} is the density, p_{ac} is the pressure, T_{ac} is absolute temperature and R is the gas constant. Here, it is assumed that the process of turbulent and molecular diffusion is fast enough for the thermodynamic variables to be taken as spatially uniform in the air chamber.

From the equation of continuity, the mass flow rate may be expressed as [27]

$$-\dot{m} = \dot{\rho}_{ac}\,V + \rho_{ac}\,\dot{V}, \tag{9}$$

where V is the time-dependent volume of air in the chamber. Its time derivative $\dot{V}$ represents the volume flow rate displaced by the motion of the inner free surface (positive for upward motion).

Since the air in the chamber is partly renovated at each wave cycle, the average temperature of the air in the chamber differs from the outer air temperature by no more than a few degrees Celsius (and much less than that in small model testing). This is why the heat exchanged across the chamber and turbine walls and at the inner air–water-free surface is very small compared with the work done by the inner free-surface motion or with the turbine work. It follows that the thermodynamic process that takes place in the inner air may be considered approximately adiabatic.

Because (i) air density is much smaller than water density, and (ii) the vertical size of the air chamber of a full-sized OWC does not exceed

a few metres, differences in potential energy in the air chamber may be neglected [27].

The first law of thermodynamics allows the time-derivative of the internal energy $U(t)$ of air in the chamber to be written as

$$\frac{\mathrm{d}U}{\mathrm{d}t} = \begin{cases} -\dot{m}_{\mathrm{out}}\,(h_{\mathrm{out}} + \frac{1}{2}v_{\mathrm{out}}^2) - p_{\mathrm{ac}}\dot{V}, & \text{if } p_{\mathrm{ac}} \geq p_{\mathrm{at}} \text{ (exhalation)} \\ \dot{m}_{\mathrm{in}}(h_{\mathrm{in}} + \frac{1}{2}v_{\mathrm{in}}^2) - p_{\mathrm{ac}}\dot{V}, & \text{if } p_{\mathrm{ac}} < p_{\mathrm{at}} \text{ (inhalation)} \end{cases} . \tag{10}$$

Here, h_{out} and h_{in} represent the specific enthalpy at the air chamber outlet during exhalation and turbine outlet during inhalation, respectively, and p_{at} is the atmospheric pressure. In the air chamber, no work is done on the fluid.

Dissipative processes due to non-zero viscosity occur in the airflow, especially in the turbine or in the turbine simulator. Because of this, the airflow is non-isentropic: the specific entropy in the air chamber exceeds the specific entropy in the atmosphere at all times [27]. The variation of specific entropy Δs_{ac} in the air chamber can be expressed as

$$\Delta s_{\mathrm{ac}} = C_v \ln\left(\frac{T_{\mathrm{ac}}}{T_{\mathrm{at}}}\right) + R \ln\left(\frac{\rho_{\mathrm{at}}}{\rho_{\mathrm{ac}}}\right), \tag{11}$$

where T_{at}, ρ_{at}, and C_v are the atmospheric air temperature, air density, and the specific heat at constant volume, respectively.

2.3. Power take-off modelling

The power take-off (PTO) system comprises an air turbine driving an electric generator. The control of its rotational speed is a major issue, and the model is described below.

2.3.1. Turbine modelling

The performance of the turbine is frequently presented in terms of dimensionless pressure head Ψ, dimensionless flow rate Φ, dimensionless power output Π and efficiency η_{turb} defined as (incompressible flow is assumed) (see [49,50])

$$\Psi = \frac{\Delta p}{\rho_{\mathrm{a,in}}\,\Omega^2\,d_{\mathrm{t}}^2}, \tag{12}$$

$$\Phi = \frac{\dot{m}_{\mathrm{turb}}}{\rho_{\mathrm{a,in}}\,\Omega\,d_{\mathrm{t}}^3}, \tag{13}$$

$$\Pi = \frac{P_{\mathrm{turb}}}{\rho_{\mathrm{a,in}}\,\Omega^3\,d_{\mathrm{t}}^5}, \tag{14}$$

$$\eta_{\mathrm{turb}} = \frac{\Pi}{\Phi\,\Psi}. \tag{15}$$

Here, it is $\Delta p = p_{\mathrm{at}}\,p^*$, where p^* is the dimensionless relative pressure oscillation in the chamber defined as

$$p^* = \frac{p}{p_{\mathrm{at}}} - 1. \tag{16}$$

In Eqs. (12), (13) and (14), Ω is the turbine rotational speed (in radians per unit time), d_{t} is the turbine rotor diameter, $\dot{m}_{\mathrm{turb}}$ is the turbine mass flow rate, and P_{turb} is the turbine power output. It should be noted that the time-scales of the OWC hydrodynamics and of the turbine aerodynamics differ by several orders of magnitude [51,52]. The absence of dynamic effects in Wells turbines is better explained in Ref. [53].

The reference density $\rho_{\mathrm{a,in}}$ is defined in stagnation conditions at the turbine entrance as

$$\rho_{\mathrm{a,in}} = \begin{cases} \rho_{\mathrm{ac}}, & \text{if } p^* > 0 \text{ (exhalation)} \\ \rho_{\mathrm{at}}, & \text{if } p^* \leq 0 \text{ (inhalation)} \end{cases} . \tag{17}$$

For sufficiently large Reynolds number $\mathrm{Re} = \Omega d_{\mathrm{t}}^2/\nu > 10^6$ and small Mach number, the performance map can be reduced to a single curve [49,50]. Figs. 2 a) and 2 b) present the dimensionless flow rate Φ, dimensionless power coefficient Π, and efficiency η, as functions of the dimensionless pressure head, Ψ for a biplane Wells turbine and a biradial air turbine.

The turbine aerodynamic power is computed from Eq. (14) as

$$P_{\mathrm{turb}} = \rho_{\mathrm{a,in}}\,\Omega^3 d_{\mathrm{t}}^5\,\Pi(\Psi). \tag{18}$$

The mass flow rate of air through the turbine and the associated specific enthalpy are turbine outputs (see Fig. 3). The specific enthalpy at the turbine's outlet $h_{\mathrm{turb}}^{\mathrm{out}}$ is defined as

$$h_{\mathrm{turb}}^{\mathrm{out}} = \begin{cases} h_{\mathrm{ac}} - \left(\frac{p_{\mathrm{ac}} - p_{\mathrm{at}}}{\rho_{\mathrm{a,in}}}\right)\eta_{\mathrm{turb}}, & \text{if } p_{\mathrm{ac}} \geq p_{\mathrm{at}} \text{ (exhalation)} \\ h_{\mathrm{at}} + \left(\frac{p_{\mathrm{ac}} - p_{\mathrm{at}}}{\rho_{\mathrm{a,in}}}\right)\eta_{\mathrm{turb}}, & \text{if } p_{\mathrm{ac}} < p_{\mathrm{at}} \text{ (inhalation)} \end{cases} , \tag{19}$$

where h_{at} and h_{ac} are the atmospheric and air chamber-specific enthalpies, respectively.

2.3.2. Electric generator and control modelling

To maximise the turbine efficiency, it shall operate at the best efficiency point Ψ_{bep}, which implies that the turbine power should comply with [56]

$$P_{\mathrm{turb}}\left(\Psi_{\mathrm{bep}}, \Omega\right) = \underbrace{\rho_{\mathrm{a,in}}\,d_{\mathrm{t}}^5\,\Pi\left(\Psi_{\mathrm{bep}}\right)}_{a_{\mathrm{bep}}=\mathrm{const}}\,\Omega^3, \tag{20}$$

and the generator power control must follow the relation

$$P_{\mathrm{ctrl}} = a_{\mathrm{bep}}\Omega^3. \tag{21}$$

In a real OWC plant subject to irregular waves, the turbine rotational speed oscillates about a more-or-less averaged value, depending on the rotational inertia of the rotating elements and on the control strategy adopted for the counter torque $T_{\mathrm{ctrl}} = P_{\mathrm{ctrl}}/\Omega$ of the generator. A control law proposed in Ref. [56] relates the instantaneous generator's counter torque to the instantaneous rotational speed Ω as

$$T_{\mathrm{ctrl}}\Omega = a\,\Omega^b, \tag{22}$$

where a and b are constants; the optimised dimensionless constant b usually takes a value of 3 [57], whereas constant a depends widely on turbine geometry and size.

An upper limit to the rotational speed could be imposed to protect the turbine and/or generator from excessive centrifugal stresses. In the case of Wells turbines, the blade tip speed should not exceed about 170 m/s.

To avoid overloading the generator, the following control law was adopted

$$P_{\mathrm{ctrl}}^{\mathrm{lim}} = \min\left(P_{\mathrm{ctrl}}, P_{\mathrm{gen}}^{\mathrm{rated}}\right), \tag{23}$$

where $P_{\mathrm{gen}}^{\mathrm{rated}}$ is the rated (maximum allowed) power of the generator.

The dynamics of the turbine and generator set can be expressed as

$$\frac{\mathrm{d}}{\mathrm{d}t}\left(\frac{1}{2}I\Omega^2\right) = P_{\mathrm{turb}} - P_{\mathrm{ctrl}}^{\mathrm{lim}}, \tag{24}$$

where Ω, I, and P_{turb} are the turbine rotational speed, the moment of inertia, and the instantaneous turbine aerodynamic power, respectively. Expanding Eq. (24) yields

$$\frac{\mathrm{d}}{\mathrm{d}t}\left(\frac{1}{2}\Omega^2\right) = \frac{1}{I}\left(\rho_{\mathrm{a,in}}\,\Omega^3 d_{\mathrm{t}}^5\,\Pi(\Psi) - P_{\mathrm{ctrl}}^{\mathrm{lim}}\right). \tag{25}$$

The air turbine type and size, the control of the turbine rotational speed, and the electric equipment's rated power have a strong effect on the power performance of an OWC [29,58].

2.3.3. The Wells turbine and the biradial turbine damping

The present work considered two different air turbine types: a Wells turbine and a biradial turbine. The Wells turbine is known to exhibit an approximately linear relationship between the pressure head coefficient, Ψ, and the flow coefficient, Φ,

$$\Psi = \mathcal{K}_{\mathrm{tW}}\Phi, \tag{26}$$

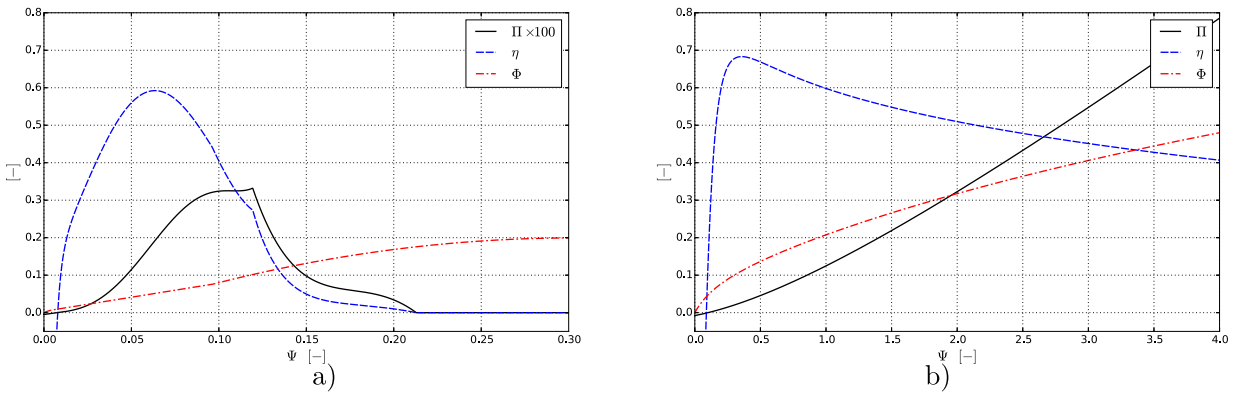

Fig. 2. Dimensionless flow rate, Φ, dimensionless power coefficient, Π, and efficiency, η, as functions of the dimensionless pressure head, Ψ, for a) the biplane Wells turbine and b) the biradial air turbine, both used in time-domain numerical simulations for the cases presented here [54,55].

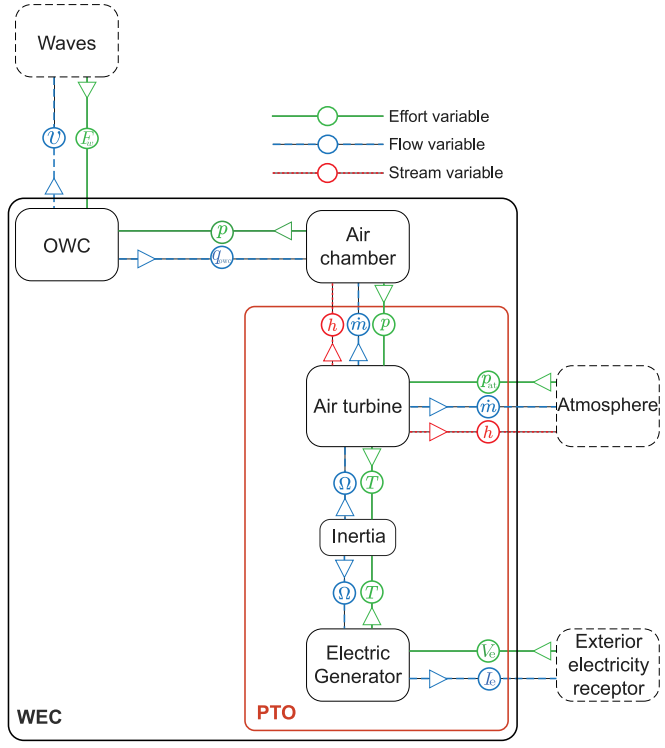

Fig. 3. Schematic representation of an OWC WEC and its connectors used in OpenModelica time-domain implementation.

where $\mathcal{K}_{tW}$ is a dimensionless constant that depends only on turbine geometry but not on turbine size, rotational speed or fluid density. This linearity is not observed when the pressure coefficient reaches values above a critical point beyond which massive flow separation occurs (aerodynamic stalling), which results in a sharp drop in efficiency to near-zero values [54] ($\Psi > 0.1$ as found in Fig. 2 a). Within the linear region, $0 \leq \Psi \leq 0.1$, the turbine damping is defined as

$$k_t = \frac{\dot{m}_{turb}}{\Delta p}\,, \tag{27}$$

and it may be computed for the Wells turbine as

$$k_{tW} = \frac{d_t}{\mathcal{K}_{tW}\,\Omega}\,. \tag{28}$$

Differently, experimental tests revealed, for the biradial turbine (and more generally for self-rectifying air turbines of impulse type), that the relationship between dimensionless values of pressure head and flow rate is fairly well-approximated by [59,60]

$$\Psi = \mathcal{K}_{tB}\,\Phi^2\,, \tag{29}$$

where $\mathcal{K}_{tB}$ is a dimensionless constant, see Fig. 2 b). From Eqs. (12) and (13) the biradial turbine damping is obtained

$$k_{tB} = d_t^2 \left(\frac{\rho_{a,in}}{\mathcal{K}_{tB}\Delta p}\right)^{1/2}\,. \tag{30}$$

From Eqs. (28) and (30), it is evident that:

1. The biradial turbine damping is strongly affected by the rotor diameter ($k_{tB} \propto d_t^2$) and weakly influenced by the rotational speed (note that Eq. (29) is an approximation).
2. The Wells turbine damping is a linear function of the rotor diameter and decreases when the rotational speed increases ($k_{tW} \propto d_t\Omega^{-1}$). It follows that, at constant rotational speed, the Wells turbine damping is independent of the available pressure.
3. The biradial turbine damping decreases when the available pressure increases ($k_{tB} \propto \Delta p^{-1/2}$).

2.3.4. Viscous dissipation terms

The model considered viscous dissipation through Morison equation-like terms, and the use of equivalent drag coefficients $C_{D,i}$ for the flow in different parts (i) of the CD-OWC. The drag force can be expressed as

$$F_D = \frac{1}{2}\rho A_{ref,i} C_{D,i} u_i(t)\left|u_i(t)\right|\,, \tag{31}$$

where $A_{ref,i}$ is a reference area associated with viscous dissipation element i, and $u_i(t)$ the velocity of concern for viscous dissipation element i. The drag coefficients were obtained from Refs. [61] and [62] and were assumed constant in the range of cases considered. Viscous dissipation elements for the CD-OWC are: the annular inlet-outlet of the totally submerged cylinder ($C_D \approx 2$), the connection of the inner and outer cylindrical ducts ($C_D \approx 1.3$), cylinder partially submerged external surface ($C_D \approx 0.7$), cylinder totally submerged external surface ($C_D \approx 0.7$), bottom of cylinder totally submerged ($C_D \approx 0.7$), cylinder totally submerged internal flow ($C_D \approx 0.06$), and cylinder partially submerged internal flow ($C_D \approx 0.07$).

2.4. Time-domain implementation in OpenModelica

The time-domain model was implemented in OpenModelica, an open-source language-based modelling and simulation environment intended for industrial and academic usage [63]. The Modelica Language is a non-proprietary, object-oriented, equation-based language to conveniently model the dynamics of complex physical systems consisting of components (objects) [64]. These objects can be, for example, mechanical, electrical, electronic, hydraulic, thermal, control, electric power or

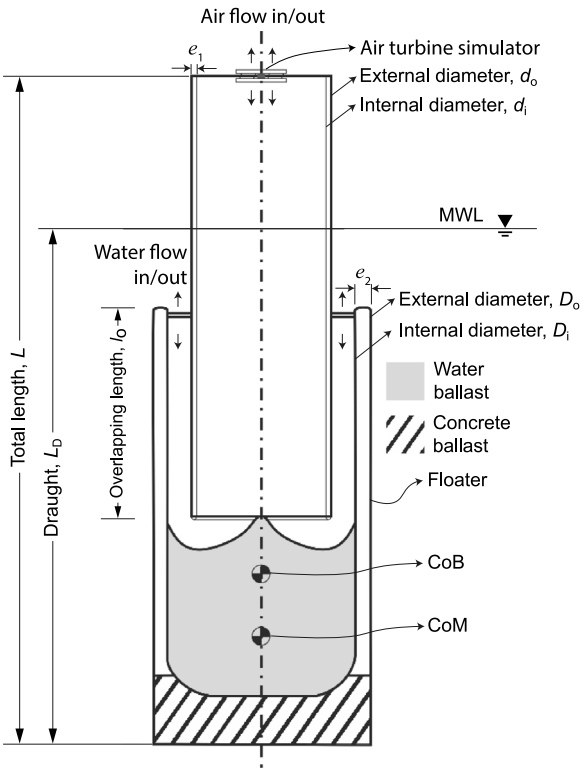

Fig. 4. Main design variables of the CD-OWC.

process-oriented components. Modelica models are described by differential, algebraic, and discrete equations [65]. Modelica language-based environments have been used in many industries [64].

The implementation of the time-domain model described in Section 2 is depicted schematically in Fig. 3, in which the main objects and their principal connectors are shown for one OWC WEC. As Modelica is an equation-based language, each component is described by its corresponding set of equations and connectors (e.g. effort, flow, or stream variable's connectors) that are used to establish the directions and interdependencies among the objects. OpenModelica was the open-source environment (editor) selected for the implementation, combined with a series of scripts in Python and C++.

Fig. 3 shows that the main effort connector variables chosen are forces, pressures, torque and voltage, while flow connector variables are velocities, volumetric flows, mass flows, rotational speeds, and current intensities. Specific enthalpy is a stream connector. The efficiency of the variable-frequency converter or other downstream electric/electronic systems were not considered in the present work. The electric generator losses were ignored.

3. Coaxial-duct OWC design

The main characteristics of the full-scale CD-OWC wave energy converter design used in this investigation are shown in Fig. 4. The full-scale design resulted from an optimisation process based on the wave climate of the western coast of Portugal, as presented in Refs. [66,67], through an optimisation approach in the frequency domain, which is similar to the one described in Ref. [66].

The hydrodynamic coefficients input to the time-domain numerical model described in Section 2 were obtained using the software WAMIT. A mesh of about 7500 source panels was considered for the CD-OWC. Computations involved 320 regular wave frequencies for the six degrees of freedom of the floating body 1 and the heave motion of body 2. A schematic representation of the discretised coaxial-duct OWC is depicted in Fig. 5, where the centre of reference is placed at the surface of the water and the centre vertical axis.

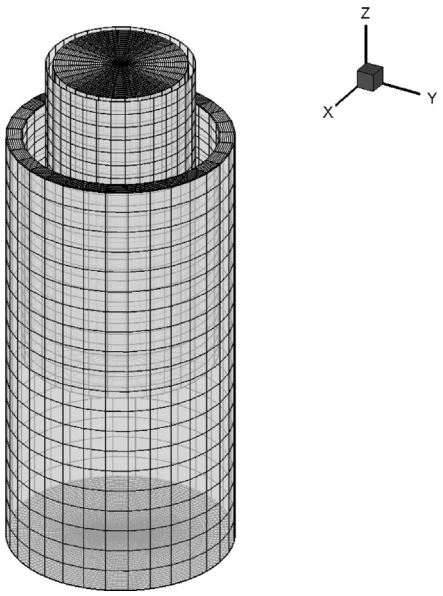

Fig. 5. Mesh representation of the CD-OWC for hydrodynamic coefficients computations.

4. Validation of numerical model

The numerical results using the model implemented in Modelica (see Section 2) are compared with experimental results in this section. The experimental results come from two different campaigns reported in Refs. [16,25,68]. The scale of the physical model tested is 1:40, with characteristics presented in greater detail in Refs. [16,25]. The tests were performed at the Portuguese National Laboratory of Civil Engineering (LNEC) at Wave Flume No. 2 (COI2). The flume is 83 m long, 3 m wide, and 3 m height. The working depth was 2 m.

Experimental testing of floating OWCs considering the spring-like compressibility effect in the OWC's air chamber requires a different scaling than the usual Froude number similitude condition (see e.g. Ref. [28]). This is one of the main difficulties when executing experiments considering these effects in the air chamber because they require an additional air volume to be part of the pneumatic chamber. This can be done easier in a fixed OWC, but in floating systems, it affects the system's dynamics due to the additional constraints in different degrees of freedom. When this additional volume is not considered, which is proportional to the square of the scaling factor and not to the cube, as when scaling using the Froude number similarity condition, it is said that the model tests are performed under incompressibility conditions. In this case, the air chamber is too stiff and does not allow the spring-like compressibility effect to behave as in full-sized OWCs.

This section presents numerical results at the model scale for incompressibility conditions, similar to what would be obtained scaling the air chamber using Froude scaling, and results considering the proper aero-thermodynamic scaling of the air chamber (i.e. considering compressibility of air in the chamber). Regarding the experimental results, one set of data was obtained considering the air chamber scaled using Froude number (incompressible case) for two wave heights under regular waves ($H = 0.05$ and 0.10 m) and an orifice of 0.01 m diameter (with a quadratic relationship between the volumetric airflow rate and the pressure drop through the orifice). Another set of data considers the proper scaling of the air chamber (compressible case) under regular waves for the same wave heights. In the latter case is worth noting that the motions of the floating device were considerably restricted due to the connection hoses and fittings (valves and others) to the additional air volume [25].

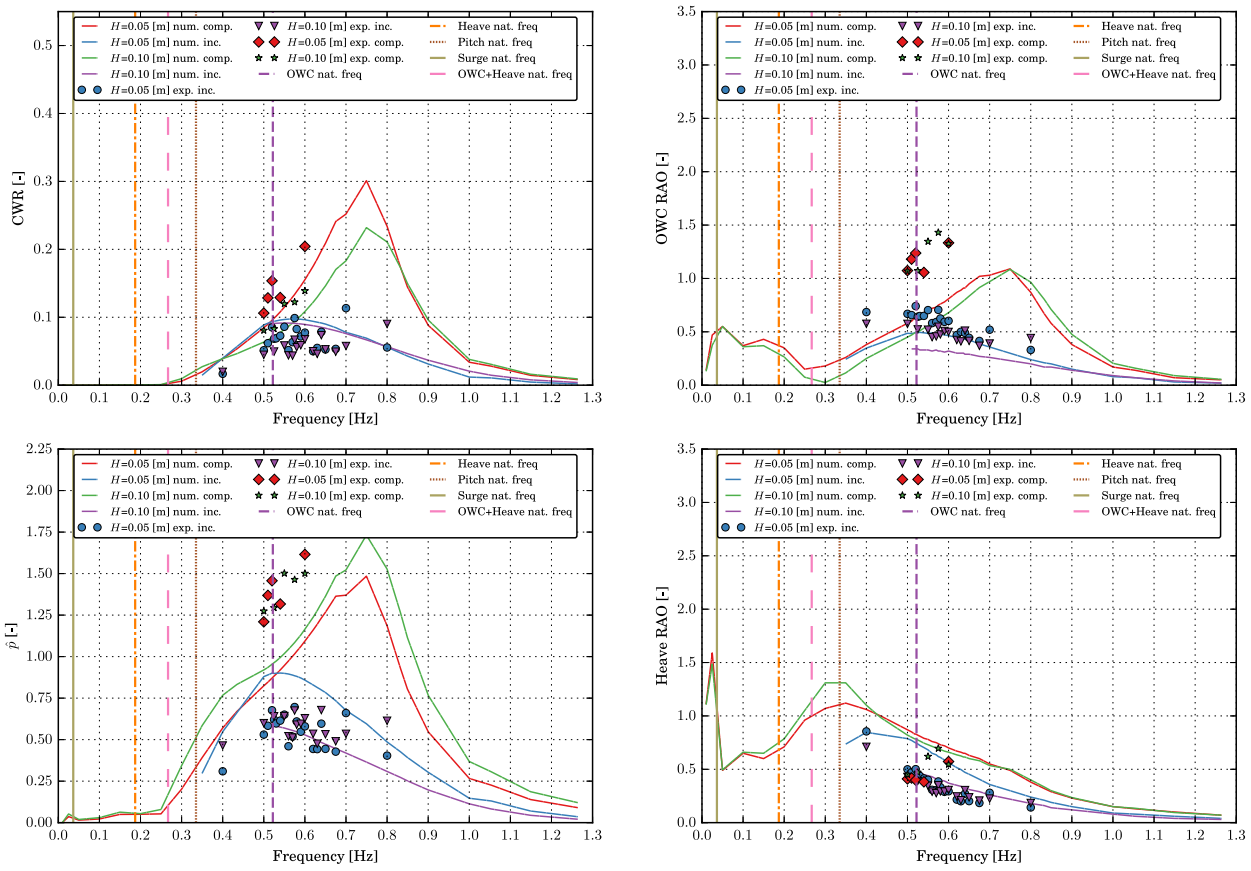

Fig. 6. Numerical results for compressible (num.) and incompressible cases (num. inc.) and experimental results for the physical model scaled using Froude similitude for an orifice of 0.01 m diameter, and waves heights of $H = 0.05$ m and $H = 0.10$ m, and different frequencies under regular waves. The figure shows the CWR, OWC RAO, dimensionless pressure $\hat{p}$, and heave RAO of the buoy. Numerical results are shown as continuous lines and experimental results with markers.

The case selected for discussion considers the floating coaxial-duct OWC with an orifice diameter of 0.01 m, simulating a biradial air turbine rotor diameter of 0.96 m at full scale. The reader is referred to Appendix A in Ref. [25] for a description of the approach undertaken for determining the equivalency between an orifice and a biradial air turbine at full scale. The regular waves with $H = 0.05$ m and $H = 0.10$ m are equivalent to $H = 2$ m and $H = 4$ m at full-scale, respectively. The case of an orifice of 0.01 m diameter, was selected because it represents a case where the spring-like compressibility effects are significant. Two other orifices were tested experimentally (0.02 m and 0.03 m diameters), but the compressibility effects were less significant as described in Ref. [25].

The capture width ratio (CWR) is the dimensionless ratio between the time-averaged pneumatic power ($\bar{P}$) and the time-averaged wave power per unit crest length ($\bar{P}_w$) multiplied by the characteristic length of the device ($D = D_o$), as follows,

$$\mathrm{CWR} = \frac{\bar{P}}{\bar{P}_w D}, \tag{32}$$

$\bar{P}$ is obtained from averaging the instantaneous power P. For regular waves, the time-averaged incident wave power per unit crest length is computed as

$$\bar{P}_w = \frac{1}{2}\rho_w g \bar{A}_w^2 c_g, \tag{33}$$

where ρ_w is the density of water, $\bar{A}_w$ is the time-averaged measured wave amplitude ($A_w = H/2$), and c_g is the group velocity [11]. The diameter of the outer duct $D_o = 0.35$ m at model scale was considered the characteristic length.

Fig. 6 shows the comparison of the numerical results under compressibility and incompressibility conditions within the air chamber, and the experimental results of the physical model scaled using Froude similarity conditions (i.e., incompressibility conditions), and aerothermodynamic scaling of the air chamber (compressibility conditions). The peak of the CWR for the compressible case and $H = 0.05$ m (red curve), for example, is much higher (about 300%) than the peak CWR obtained under incompressibility conditions. Furthermore, the incompressible curve is much flatter with the relatively larger values of CWR towards the natural frequency of the OWC (about 0.526 Hz [16]). Indeed, the experimental results for the incompressible case are closer, as expected, to the incompressible numerical curves. In contrast, the compressible case experimental results are considerably different than the experimental incompressible case and closer to the numerical compressible case curves, but still with noticeable differences. Remember that the extra volume of air connected to the model significantly alters the dynamic of the experimental case considering compressibility. It is, certainly, one important source of differences.

These results support the idea of having significant power output differences when spring-like compressibility effects in the air chamber are disregarded, especially in air chambers with PTOs inducing high damping. The compressibility factor presented in Ref. [25] may represent a measure to identify when compressibility effects are more considerable in experimental or numerical campaigns.

The OWC and heave RAO are defined as OWC RAO = $\bar{A}_{owc}/\bar{A}_w$, and heave RAO = $\bar{A}_{heave}/\bar{A}_w$, respectively. $\bar{A}_{owc}$, $\bar{A}_{heave}$, and $\bar{A}_w$ represent the mean amplitudes of the internal mass of water (OWC), the device's heave motion, and the wave amplitute, respectively.

The OWC and heave RAOs shown in Fig. 6 evidence that the experimental incompressible results follow the trend of the incompressible numerical ones. Despite the excessive restriction in the device's motion in the compressible experimental results, it is evident a difference

Table 1
Dimensions of the CD-OWC full-scale prototype. See Fig. 4 for the meaning of the symbols.

Parameter	Full-scale
L [m]	43.0
L_D [m]	33.0
l_o [m]	13.0
D_o [m]	14.0
D_i [m]	12.0
d_o [m]	9.2
d_i [m]	8.2
e_1 [m]	0.5
e_2 [m]	1.1
M [kg]	1.818×10^6
I [kg m^2]	288.1×10^6
CoB to MWL [m]	22.6
CoM to MWL [m]	26.3
Air chamber volume V (Froude) [m^3]	528.1

between both sets of experimental data (i.e. compressible versus incompressible cases). In Ref. [25], a more equivalent comparison was made between compressible and incompressible cases, which supports this observation.

The peaks of the RAOs occur at different frequencies when comparing the compressible and incompressible numerical results. It means the shift of the OWC RAO peak under incompressibility conditions is to the left (lower frequencies) relative to the peak for the compressible numerical results and aligned with what was found experimentally. In contrast, the heave RAO curve of the buoy for the incompressible case is flatter and seems to shift slightly to the right (higher frequencies) compared to the compressible case. It is believed that the different phases between the OWC elevation and the heave elevation of the buoy provoked by the different damping and stiffness in the air chamber affect the RAOs, being the more sensitive the OWC RAO. It is also evident that compressibility effects affect the system's motion.

The dimensionless pressure is defined as

$$\hat{p} = \frac{\bar{p}}{\rho_w g \bar{A}_w}, \tag{34}$$

where $\bar{A}_w$ is the mean amplitude of the waves, ρ_w represents the density of water, and g is the gravity acceleration constant on earth.

In Fig. 6, the highest dimensionless pressure ($\hat{p}$) peak is shifted to the left as occurs with the peak in the CWR and OWC RAO for the incompressible numerical case compared to the compressible one. The numerical incompressible case pressure seems to overestimate the experimental results for $H = 0.05$ m. This may be due to higher losses within the actual physical model and mooring line forces oversimplified in the numerical model.

The overall trend agrees despite some differences between the experimental and numerical results for the incompressible cases. Regarding the compressible case results, it can be said that based on the over-restricted motions of the model presented in Ref. [25], the trend of having higher CWRs in compressible results when compared to the incompressible agrees, and that differences increase with an increase in frequency.

In summary, significant differences in floating OWC dynamics occur between compressible and incompressible cases. These differences affect the hydrodynamics of the system inducing effects over displacement RAOs, the pressure within the chamber, and the capture width ratio. In addition, proper PTO optimisation and selection must involve realistic compressible conditions within the air chamber, and performing this task disregarding compressibility may induce misleading results for the PTO. It also represents a necessary knowledge to select appropriate air turbine systems for tuning a specific design of OWC to be deployed in different potential locations (and conditions).

5. Results and discussion

5.1. Chamber volume influence and compressibility effects

The chamber volume influence and compressibility effects have been explored in several works. Nevertheless, there are still concerns and doubts about how the underlying mechanisms can be exploited or further used to effectively broaden the bandwidth of high extraction efficiency. A better knowledge of the phenomenon is expected to close the gap.

The results presented in this section concern the same OWC design described in Section 3 at full scale but with different air chamber volumes represented in terms of the air chamber height h_a. The dimensionless wave frequency is defined as $\omega^* = \omega\sqrt{D_o/g}$ with $D_o = 14$ m (see Table 1). Fig. 7 presents the variation of CWR for different air chamber heights for the coaxial-duct OWC equipped with biradial air turbines of 0.96 m and 2.93 m diameters. It can be observed that for the largest turbine, there are no perceptible variations in the CWR values. In contrast, there is a substantial variation in the CWR values per air chamber height for the smaller turbine. Indeed, the compressibility effects are more significant when using the 0.96 m rotor diameter turbine. The smaller and stiffer chambers present flatter curves, while the 10 m and the 15 m air chambers present more differentiated peaks. Clear peak shifts in CWR values exist between the air chambers' results. Other authors [69,70] already pointed out that the PTO damping and the chamber size were important parameters for tuning a fixed OWC system to a specific range of sea states. Some particular points were identified and explained in the next section.

5.2. Critical points of compressibility effects

A series of critical points have been identified in previous works for which the compressibility effects are negligible or at least similar. Compressible and incompressible air chamber models produce similar results when negligible effects are present. This was predicted theoretically for the first time for a fixed OWC in Ref. [27], and further studied theoretically and compared with experimental data also for a fixed OWC in Ref. [28], supported by data reported in Ref. [35]. It was shown for the fixed OWC case study that critical points with negligible compressibility effects are located between the peaks of maximum CWR of compressible and incompressible CWR curves [28]. In the same work, the model could predict the critical wave frequency when compared with the experimental results presented in Ref. [35]. Furthermore, similar observations were made in another recent work focused on other aspects of pile-supported OWC breakwaters and their wave field interactions [71].

It is worth noting that regarding the critical points described in Ref. [28], a critical wave frequency was shown to be independent of incident wave amplitude and turbine simulator type and size (i.e., orifice used in experimental testing to simulate an impulse air turbine). Moreover, it was shown theoretically that the critical wave frequency depends only on the radiation susceptance function and the air chamber volume. However, the reader, at this point, should be aware that the objective of the work just described was a correction to experimental results that accounts for air compressibility. Consequently, extensive analysis considering different air chamber volumes was not addressed.

In practice, when project developers need to design OWCs and select the most appropriate characteristics for the OWC system, a more general overview of the system's behaviour is required. Hereinafter, it is shown that various critical point types may be expected in the design and analysis of OWCs. One of these points is named as *Equicompressum Nullum* critical point, which is mostly independent of the air chamber volume and corresponds to zero compressibility effects, as represented in Fig. 7(a) by a black circle for the CD-OWC.

Nevertheless, in the same figure, additional critical points may be observed for any air chamber volume using the same PTO, which can be

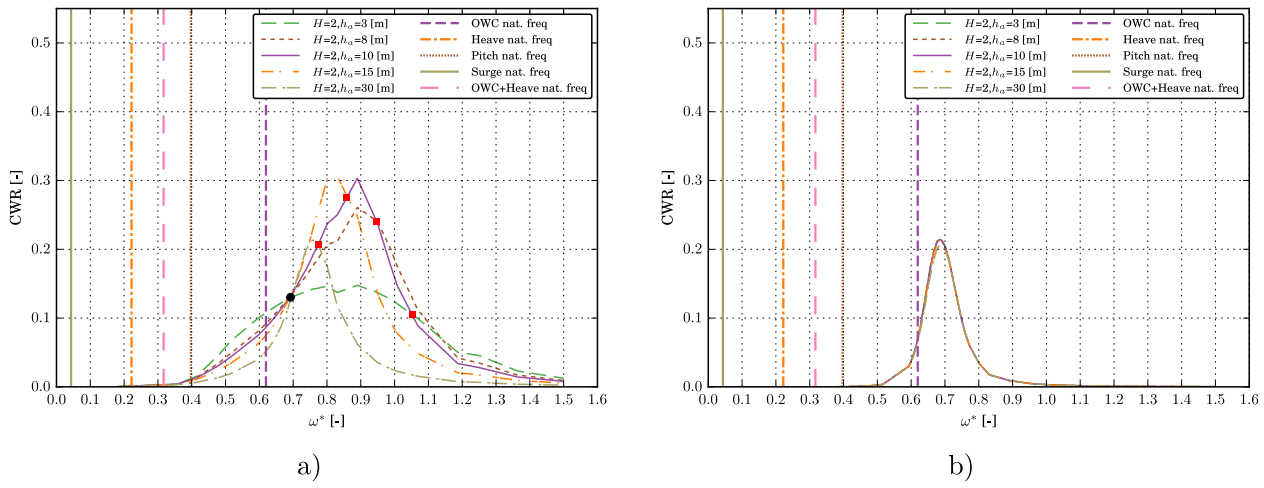

Fig. 7. Numerical results for the CWR and different air chamber heights for the floating coaxial-duct OWC for biradial air turbines of a) 0.96 m and b) 2.93 m diameters, under regular waves with $H = 2$ m. The black circle and the red squares in a) represent critical points, and they are discussed in Section 5.2.

named *Equicompressum* critical points. See, for example, the red squares represented in Fig. 7(a), for a selected air chamber height of 10 m. These points represent the intersections of different CWR spectra as a function of the air chamber volume. In contrast with the *Equicompressum Nullum* critical point, these points have compressibility effects associated, but the relative differences in CWR between two or more spectra are coincident. Therefore, the knowledge of these points may have important implications in the design and control of oscillating-water-column wave energy converters.

The reader should be aware now that for a given hydrodynamic design of OWC and a PTO, one curve of a specific air chamber volume size can have one or more critical points (see Fig. 7 (a)). Furthermore, both types of points represent inflexion points that separate the negative from positive (or positive from negative) effects of compressibility.

5.3. Fixed and floating CD-OWC: Chamber height influence and compressibility effects

Numerical results for a fixed and a floating CD-OWC are presented in Fig. 8. The CWR, OWC RAO, and dimensionless pressure $\hat{p}$ are shown for different air chamber volumes, indicated as air chamber height for the same cross-chamber section. The lowest value of the air chamber approaches incompressible conditions; compressibility effects vary with the chamber height. The figure considers a biradial air turbine of 0.96 m rotor diameter and regular wave height of 2 m at full scale.

It can be observed that the *Equicompressum Nullum* critical points for the fixed and floating case are slightly different. This is believed to be associated with the coupled hydrodynamic interaction of the floating system in different degrees of freedom and moorings. Considering the floating device, for example, the relative heave motion between the vertical displacement of the physical device and the internal water surface (assumed as a thin piston) is what effectively displaces the air in and out of the air chamber. In contrast, in the fixed OWC with zero displacements, the only source of reciprocating motion is the internal free surface of the water. Therefore, differences were expected between the fixed and floating devices. Nevertheless, they are small.

The *Equicompressum Nullum* critical point for the fixed device occurs very close to the dimensionless natural frequency of the internal mass of water (at about $\omega^* = 0.625$ where the maximum CWR occurs for the fixed device under incompressibility conditions and a large diameter turbine), while in the floating version occurs at about $\omega^* = 0.682$ where the maximum capture width ratio without significant compressibility effects occurs (see Fig. 7(b)).

The fixed device presents slightly higher values of CWR around the peaks, induced mainly by the absence of influence of the device motions. Remember that the CWR in the floating device is influenced by the relative motion between the device and the displacement of the internal OWC, as aforementioned. Furthermore, it can be observed that for a specific geometry of a CD-OWC (fixed or floating), the variation in the air chamber volume changes: (i) the bandwidth of CWR performance as a function of frequencies, which implies changes in symmetry and steepness, (ii) the magnitude of CWR peaks, (iii) the peaks of CWR curves as a function of frequencies, and (iv) the relative magnitude of positive to negative (or negative to positive) compressibility effects between transition regions demarked by the critical points.

The larger the air chamber height, the larger the OWC motions due to fewer restrictions to the displacement of the water–air interface. In contrast, it can be seen that the pressure oscillation amplitudes (presented as dimensionless pressure amplitudes) can get optimum CWR values at different frequencies as a function of air chamber volume. In other words, for a given frequency, an optimum air chamber volume will give the highest CWR at that frequency.

5.4. Annual mean power and turbine selection

This section presents the effect of the turbine size on the turbine power output for a coaxial-duct OWC at full scale for an air chamber height of 10 m. The wave climate in Table 2, representative of the western coast of Portugal, was used to assess the optimal turbine rotor diameter for both a biradial air turbine and Wells air turbine, with characteristic curves presented in Fig. 2. The numerical model was used to evaluate different rotor diameters of each turbine for wave climates 1 to 12 from Table 2. The two most energetic sea states (and less frequent) with significant wave heights 6.99 m and 8.17 m were ignored in the computations.

The influence of the turbine size on the power output is presented in Fig. 9 considering a 100% efficient electric generator. The mean annual pneumatic power available to the turbine, turbine output power, CWR, and turbine efficiency are shown. These values represent weighted averages obtained from the mean values for sea states 1 to 12 weighted by their probability of occurrence. It can be observed that the optimum rotor diameter for the biradial air turbine is about 1.50 m, and for the Wells turbine is about 1.75 m. Lower diameters of the Wells turbine will induce stall conditions and excessive rotational speeds, resulting in lower turbine availability. The control implemented for all simulations in this work was rotational speed control to keep the turbines working close to their best efficiency points. No additional control mechanisms were adopted. The Wells turbine presents more difficulties in controlling than the biradial air turbine. Other control mechanisms should be considered in actual implementations; valves are

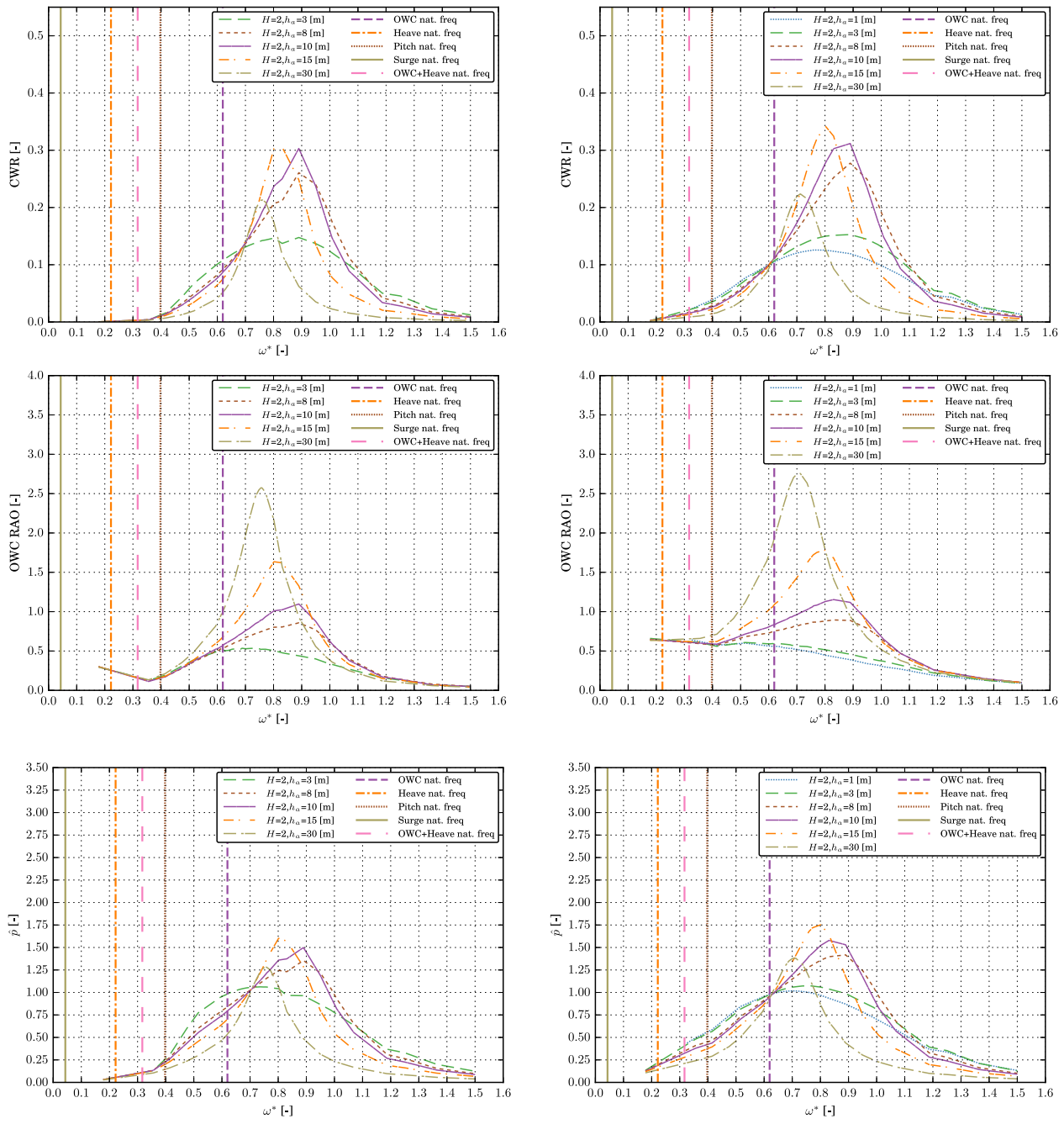

a) Floating CD-OWC. b) Fixed CD-OWC.

Fig. 8. Numerical results for the CD-OWC with a biradial air turbine of 0.96 m diameter under regular waves of height $H = 2$ m, and different dimensionless frequencies for various air chamber heights. It is shown the CWR, OWC RAO, and dimensionless pressure $\hat{p}$ for a) a floating and b) a fixed CD-OWC. Fig. 7a) is reproduced here for ease of comprehension.

usually used to control the volumetric airflow and pressure within the air chamber. Nevertheless, the Wells turbine usually is less expensive than the biradial air turbine due to its simplicity.

Fig. 10 shows the selected turbine sizes' power distributions determined through the aforementioned parametric analysis. With the knowledge of the wave climate of specific locations and the occurrences of sea states, these power distributions can be used to estimate the averaged annual power of the turbine in any place.

5.5. Applications potential for the CD-OWC

Some niche markets have been identified for stand-alone applications of the CD-OWC or similar WECs with similar power levels. One of these markets is the ocean observation and navigation market, which has current power level needs of hundreds of watts. Still, it is expected to increase as these systems evolve into more complex observational and navigation aid stations. As a result, their power level requirements may pass to be in the order of tens of kW. It was highlighted about ten years ago that this market had a value of about $16 billion [72].

Another market identified was associated with underwater vehicle hosting and charging, representing another application with a power

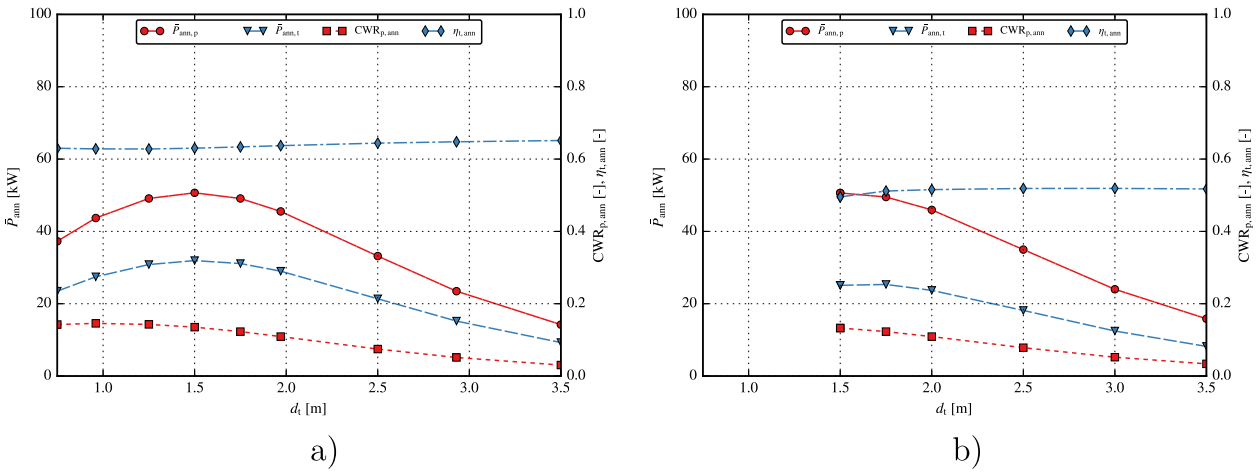

Fig. 9. Mean annual pneumatic power $\bar{P}_{ann,p}$, mean annual turbine power $\bar{P}_{ann,t}$, mean annual pneumatic capture width ratio $CWR_{p,ann}$, and mean annual turbine efficiency $\eta_{t,ann}$ versus turbine's rotor diameter for a) a biradial air turbine, and b) a Wells turbine. The results shown are for the Portuguese's west coast reference sea states and were obtained through numerical simulations.

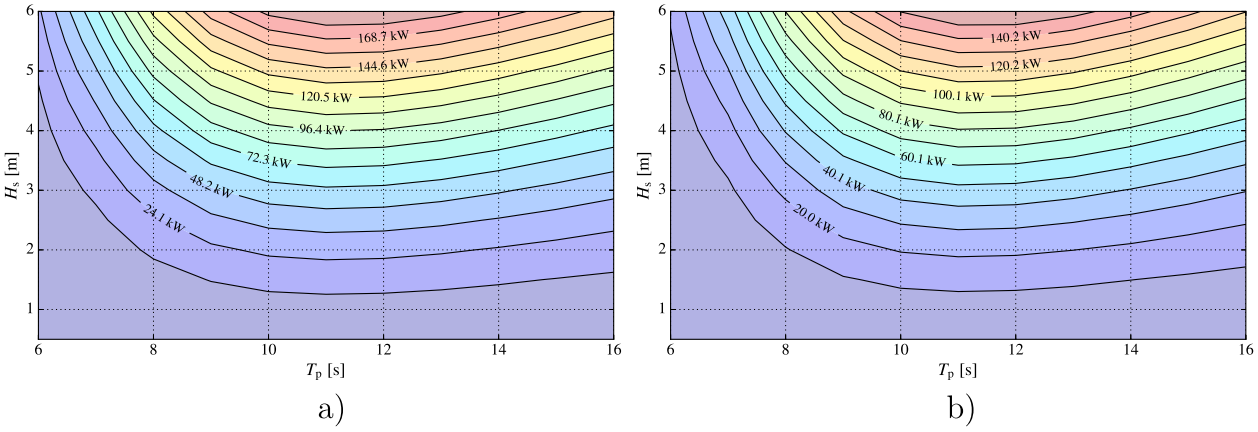

Fig. 10. Turbine power distributions for a) biradial air turbine with a rotor diameter of 1.50 m, and b) Wells turbine with a rotor diameter of 1.75 m.

Table 2
Characteristic wave climate off the western coast of Portugal. Each sea state n of the wave climate is defined by the significant wave height, H_s, energy period, T_e, and probability of occurrence, ξ_n [66].

n	H_s [m]	T_e [s]	ξ_n [%]
1	1.10	5.49	7.04
2	1.18	6.50	12.35
3	1.23	7.75	8.17
4	1.88	6.33	11.57
5	1.96	7.97	20.66
6	2.07	9.75	8.61
7	2.14	11.58	0.59
8	3.06	8.03	9.41
9	3.18	9.93	10.07
10	3.29	11.80	2.57
11	4.75	9.84	4.72
12	4.91	12.03	2.81
13	6.99	11.69	1.01
14	8.17	13.91	0.39

level requirement in the order of a few kilowatts. This market had a global value of $2.6 billion in 2017, which was expected to double in less than ten years [72].

Offshore aquaculture and marine algae production are another interesting set of applications for the coaxial-duct OWC. The power level requirements for the applications range from tens of kilowatts to a few hundred kilowatts in small-to-medium farms [72]. The global aquaculture products in 2018 represented about 155 million tonnes with a market value close to $264 billion. The global marine plant production in the same year represented about 32.4 million tonnes with a market value of around $13.3 billion [73]. The coaxial-duct OWC may represent one of the solutions for these applications. One or more devices can be installed around the aquaculture farm to provide the power required for the operations. Nevertheless, as in all applications, specific project conditions need to be assessed to study the feasibility of incorporating one or more coaxial-duct OWCs. Fig. 11 shows some of these applications for the coaxial-duct OWC.

Other applications with power levels in the order of tens of kilowatts may be satisfied with one or more devices, such as defence and surveillance systems involving radar and intruders monitoring, isolated power systems for community micro-grids, ocean pollution clean-up, and others. In any case, detailed project assessments need to be developed to determine their feasibility.

6. Conclusions

This work presents a new non-linear model for oscillating-water-column (OWC) wave energy converters (WECs) implemented in the object-oriented language Modelica to assess their performance in the time domain. It was found to be a powerful wave-to-wire conversion tool. The study's objective was to evaluate the spring-like air compressibility effects known to be significant in full-sized OWC WECs. Such effects should not be ignored in wave energy converter's design.

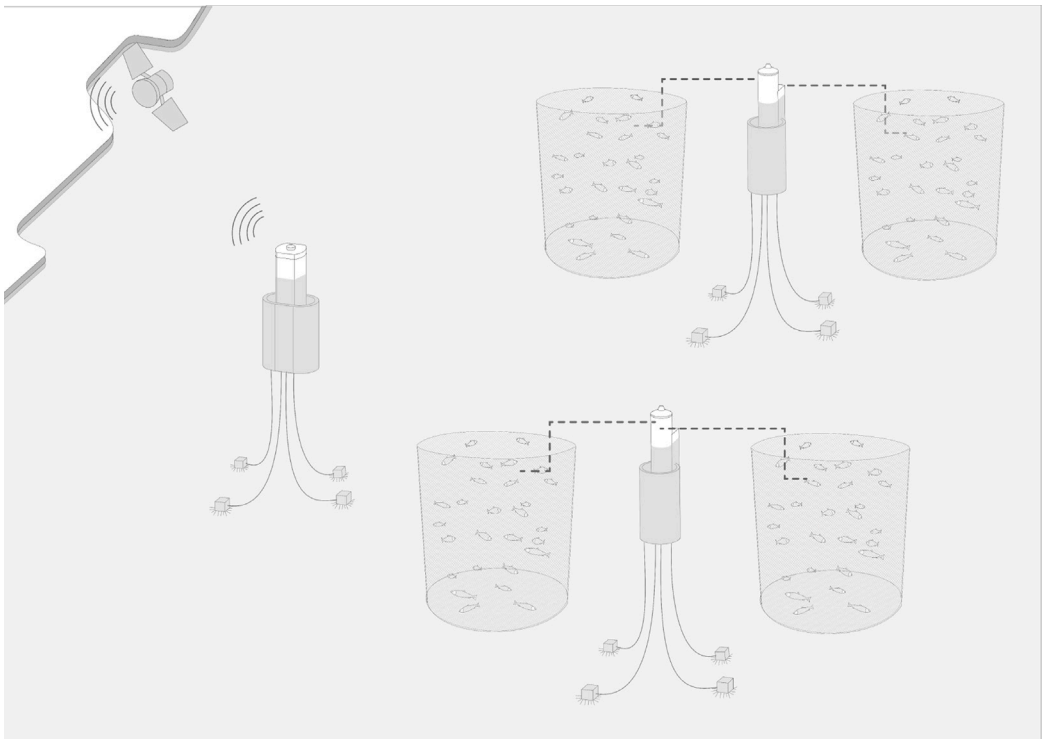

Fig. 11. Schematic representation of applications for the coaxial-duct OWC. Oceanographic monitoring and offshore aquaculture are shown as examples.

Numerical and experimental results showed that air compressibility might significantly affect the OWC performance. Depending on wave frequency, the air compressibility reduces or increases the energy the system absorbs. The relative magnitude of positive to negative (or negative to positive) compressibility effects between transition regions is separated by critical points. These were categorised as *Equicompressum Nullum* critical point, which is mostly independent of the air chamber volume and corresponds to zero compressibility effects; and *Equicompressum* critical points, which represent the intersections of different CWR curves, as a function of the air chamber volume. Knowing these critical points brings important implications for the control of OWCs.

Compressibility effects in fixed and floating versions of the same coaxial-duct OWC were analysed. Results showed slightly different behaviours; the fixed OWC exhibited slightly better performances around CWR peaks, due to the additional modes of motion and forces in the floating configuration. It was also found that the additional degrees of freedom in the floating system slightly affect the frequencies associated with the critical points.

Furthermore, a methodology for selecting air turbines for OWC WECs was presented for a coaxial-duct OWC design and a location off the western coast of Portugal. Finally, applications for the system power output level were also briefly discussed.

Implementing OWC numerical models using Modelica might help develop and design OWC converters due to this language's potential for modularity and flexibility, allowing for modelling much more complex configurations of oscillating-water-columns and offshore energy farms.

CRediT authorship contribution statement

J.C.C. Portillo: Model formulation and implementation, Experiment development, Formal analysis, Methodology, Investigation, Validation, Writing – original draft, Visualisation. **L.M.C. Gato:** Conceptualisation, Model formulation, Formal analysis, Methodology, Funding acquisition, Supervision, Validation, Writing – review & editing, Project administration. **J.C.C. Henriques:** Conceptualisation, Model formulation, Formal analysis, Methodology, Investigation, Software, Validation, Writing – review & editing. **A.F.O. Falcão:** Formal analysis, Methodology, Writing – review & editing.

Declaration of competing interest

The authors declare that they have no known competing financial interests or personal relationships that could have appeared to influence the work reported in this paper.

Acknowledgements

This work was funded by the Portuguese Foundation for Science and Technology (FCT) through IDMEC, under LAETA, project UIDB/50022/2020. The authors thank the Portuguese National Laboratory of Civil Engineering (LNEC), especially Dr Juana Fortes, for the support, receptivity and permission to use the wave flume for the experiments reported in this work. The authors also acknowledge the collaboration of the University of Plymouth for lending the 1:40-scale coaxial-duct model constructed under the EU H2020 Wave Energy Transition to Future by Evolution of Engineering and Technology (WETFEET) project with grant agreement No 641334.

References

[1] United Nations, The Paris agreement, 2023, URL https://unfccc.int/process-and-meetings/the-paris-agreement/the-paris-agreement. (Accessed 2 March 2023).
[2] European Council, Fit for 55, 2023, https://www.consilium.europa.eu/en/policies/green-deal/fit-for-55-the-eu-plan-for-a-green-transition/. (Accessed 2 March 2023).
[3] International Energy Agency, Policies database, 2023, https://www.iea.org/policies/about. (Accessed 2 March 2023).
[4] United Nations, Blue economy: oceans as the next great economic frontier, 2023, https://unric.org/en/blue-economy-oceans-as-the-next-great-economic-frontier/. (Accessed 2 March 2023).
[5] European Commission, European green deal: Developing a sustainable blue economy in the European union, 2023, https://ec.europa.eu/commission/presscorner/detail/en/qanda_21_2346. (Accessed 2 March 2023).
[6] S. Barstow, G. Mørk, D. Mollison, J. Cruz, The wave energy resource, in: J. Cruz (Ed.), Ocean Wave Energy: Current Status and Future Prespectives, Springer, Berlin, 2008, pp. 93–132, http://dx.doi.org/10.1007/978-3-540-74895-3_4.
[7] J.P. Kofoed, The wave energy sector, in: A. Pecher, J.P. Kofoed (Eds.), Handbook of Ocean Wave Energy, Springer International Publishing, Cham, 2017, pp. 17–42, http://dx.doi.org/10.1007/978-3-319-39889-1_2.

[8] B. Drew, A.R. Plummer, M.N. Sahinkaya, A review of wave energy converter technology, Proc. Inst. Mech. Eng. A 223 (2009) 882–902, http://dx.doi.org/10.1243/09576509JPE782.

[9] A.F.O. Falcão, Wave energy utilization: A review of the technologies, Renew. Sustain. Energy Rev. 14 (2010) 899–918, http://dx.doi.org/10.1016/j.rser.2009.11.003.

[10] I. López, J. Andreu, S. Ceballos, M. de Alegria, I. Kortabarria, Review of wave energy technologies and the necessary power-equipment, Renew. Sustain. Energy Rev. 22 (2013) 413–434, http://dx.doi.org/10.1016/j.rser.2013.07.009.

[11] D. Greaves, 3. Wave energy technology, in: D. Greaves, G. Iglesias (Eds.), Wave and Tidal Energy, Wiley, Hoboken, NJ, 2018, pp. 52–104.

[12] U.S. Department of Energy, Advancing commercial viability of wave energy technologies can accelerate a carbon-free grid, 2023, https://www.energy.gov/articles/doe-announces-25-million-cutting-edge-wave-energy-research. (Accessed 2 March 2023).

[13] EuropeWave, Welcome to EuropeWave, 2023, https://www.europewave.eu/. (Accessed 2 March 2023).

[14] V. Heller, 8.04 - Development of wave devices from initial conception to commercial demonstration, in: A. Sayigh (Ed.), Comprehensive Renewable Energy, Elsevier, Oxford, 2012, pp. 79–110, http://dx.doi.org/10.1016/B978-0-08-087872-0.00804-0.

[15] P. Vigars, K. Lee, S. Shin, B. Ekergard, M. Leijon, Y. Torre-Enciso, D. Marina, D. Greaves, 12. Project development, in: D. Greaves, G. Iglesias (Eds.), Wave and Tidal Energy, Wiley, Hoboken, NJ, 2018, pp. 533–586.

[16] J.C.C. Portillo, K.M. Collins, R.P.F. Gomes, J.C.C. Henriques, L.M.C. Gato, B.D. Howey, M.R. Hann, D.M. Greaves, A.F.O. Falcão, Wave energy converter physical model design and testing: The case of floating oscillating-water-columns, Appl. Energy 278 (2020) 115638, http://dx.doi.org/10.1016/j.apenergy.2020.115638.

[17] T.V. Heath, A review of oscillating water columns, Phil. Trans. R. Soc. A 370 (1959) (2012) 235–245, http://dx.doi.org/10.1098/rsta.2011.0164.

[18] G. Malara, F. Arena, Analytical modelling of an U-Oscillating Water Column and performance in random waves, Renew. Energy 60 (2013) 116–126, http://dx.doi.org/10.1016/j.renene.2013.04.016.

[19] A.F.O. Falcão, J.C.C. Henriques, Oscillating-water-column wave energy converters and air turbines: A review, Renew. Energy 85 (2016) 1391–1424, http://dx.doi.org/10.1016/j.renene.2015.07.086.

[20] N. Delmonte, D. Barater, F. Giuliani, P. Cova, G. Buticchi, Review of oscillating water column converters, IEEE Trans. Ind. Appl. 52 (2) (2016) 1698–1710, http://dx.doi.org/10.1109/TIA.2015.2490629.

[21] A.A. Wells, Fluid driven rotary transducer, in: British Patent Spec No. 1595700, 1976.

[22] R. Curran, L.M.C. Gato, The energy conversion performance of several types of Wells turbine designs, Proc. Inst. Mech. Eng. A 221 (1997) 133–145, http://dx.doi.org/10.1243/0957650971537051.

[23] A. Scialò, J.C.C. Henriques, G. Malara, A.F.O. Falcão, L.M.C. Gato, F. Arena, Power take-off selection for a fixed U-OWC wave power plant in the Mediterranean Sea: The case of Roccella Jonica, Energy 215 (2021) 119085, http://dx.doi.org/10.1016/j.energy.2020.119085.

[24] A.F.O. Falcão, J.C.C. Henriques, Model-prototype similarity of oscillating-water-column wave energy converters, Int. J. Marine Energy 6 (2014) 18–34, http://dx.doi.org/10.1016/j.ijome.2014.05.002.

[25] J.C.C. Portillo, J.C.C. Henriques, L.M.C. Gato, A.F.O. Falcão, Model tests on a floating coaxial-duct OWC wave energy converter with focus on the spring-like air compressibility effect, Energy (2022) 125549, http://dx.doi.org/10.1016/j.energy.2022.125549.

[26] A.J.N.A. Sarmento, A.F. de O. Falcão, Wave generation by an oscillating surface-pressure and its application in wave-energy extraction, J. Fluid Mech. 150 (1985) 467–485, http://dx.doi.org/10.1017/S0022112085000234.

[27] A.F.O. Falcão, J.C.C. Henriques, The spring-like air compressibility effect in oscillating-water-column wave energy converters: Review and analyses, Renew. Sustain. Energy Rev. 112 (2019) 483–498, http://dx.doi.org/10.1016/j.rser.2019.04.040.

[28] A.F.O. Falcão, J.C.C. Henriques, R.P.F. Gomes, J.C.C. Portillo, Theoretically based correction to model test results of OWC wave energy converters to account for air compressibility effect, Renew. Energy 198 (2022) 41–50, http://dx.doi.org/10.1016/j.renene.2022.08.034.

[29] A.F.O. Falcão, P.A.P. Justino, OWC wave energy devices with air flow control, Ocean Eng. 26 (12) (1999) 1275–1295, http://dx.doi.org/10.1016/S0029-8018(98)00075-4.

[30] W. Sheng, R. Alcorn, A.W. Lewis, On thermodynamics in the primary power conversion of oscillating water column wave energy converters, J. Renew. Sustain. Energy 5 (2013) 023105.

[31] W. Sheng, A. Lewis, Wave energy conversion of oscillating water column devices including air compressibility, J. Renew. Sustain. Energy 8 (5) (2016) 054501, http://dx.doi.org/10.1063/1.4963237.

[32] A. Elhanafi, G. Macfarlane, A. Fleming, Z. Leong, Scaling and air compressibility effects on a three-dimensional offshore stationary OWC wave energy converter, Appl. Energy 189 (2017) 1–20, http://dx.doi.org/10.1016/j.apenergy.2016.11.095.

[33] A.S. Dimakopoulos, M.J. Cooker, T. Bruce, The influence of scale on the air flow and pressure in the modelling of oscillating water column wave energy converters, Int. J. Marine Energy 19 (2017) 272–291, http://dx.doi.org/10.1016/j.ijome.2017.08.004.

[34] H. Martins-Rivas, C.C. Mei, Wave power extraction from an oscillating water column along a straight coast, Ocean Eng. 36 (6) (2009) 426–433, http://dx.doi.org/10.1016/j.oceaneng.2009.01.009.

[35] I. López, R. Carballo, F. Taveira-Pinto, G. Iglesias, Sensitivity of OWC performance to air compressibility, Renew. Energy 145 (2020) 1334–1347, http://dx.doi.org/10.1016/j.renene.2019.06.076.

[36] I. Simonetti, L. Cappietti, H. Elsafti, H. Oumeraci, Evaluation of air compressibility effects on the performance of fixed OWC wave energy converters using CFD modelling, Renew. Energy 119 (2018) 741–753, http://dx.doi.org/10.1016/j.renene.2017.12.027.

[37] R.A.A.C. Gonçalves, P.R.F. Teixeira, E. Didier, F.R. Torres, Numerical analysis of the influence of air compressibility effects on an oscillating water column wave energy converter chamber, Renew. Energy 153 (2020) 1183–1193, http://dx.doi.org/10.1016/j.renene.2020.02.080.

[38] M.R. Mia, M. Zhao, H. Wu, A. Munir, Numerical investigation of scaling effect in two-dimensional oscillating water column wave energy devices for harvesting wave energy, Renew. Energy 178 (2021) 1381–1397, http://dx.doi.org/10.1016/j.renene.2021.07.011.

[39] S. Dai, S. Day, Z. Yuan, H. Wang, Investigation on the hydrodynamic scaling effect of an OWC type wave energy device using experiment and CFD simulation, Renew. Energy 142 (2019) 184–194, http://dx.doi.org/10.1016/j.renene.2019.04.066.

[40] F. Cambuli, T. Ghisu, I. Virdis, P. Puddu, Dynamic interaction between OWC system and Wells turbine: A comparison between CFD and lumped parameter model approaches, Ocean Eng. 191 (2019) 106459, http://dx.doi.org/10.1016/j.oceaneng.2019.106459.

[41] J.C.C. Henriques, J.C.C. Portillo, W. Sheng, L.M.C. Gato, A.F.O. Falcão, Dynamics and control of air turbines in oscillating-water-column wave energy converters: Analyses and case study, Renew. Sustain. Energy Rev. 112 (2019) 571–589, http://dx.doi.org/10.1016/j.rser.2019.05.010.

[42] T. Setoguchi, M. Takao, K. Kaneko, Hysteresis on Wells turbine characteristics in reciprocating flow, Int. J. Rotating Mach. 4 (1998) 867414, http://dx.doi.org/10.1155/S1023621X98000025.

[43] J.-M. Zhan, Q. Fan, W.-Q. Hu, Y.-J. Gong, Hybrid realizable k-ϵ laminar method in the application of 3D heaving OWCs, Renew. Energy 155 (2020) 691–702, http://dx.doi.org/10.1016/j.renene.2020.03.140.

[44] J.C.C. Portillo, J.C.C. Henriques, R.P.F. Gomes, L.M.C. Gato, A.F.O. Falcão, On the array of wave energy converters: The case of the coaxial-duct OWC, in: Proceedings of the 37th International Conference on Ocean, Offshore and Arctic Engineering, Madrid, Paper No. OMAE2018-78022, 2018.

[45] J.C.C. Portillo, A.F.O. Falcão, J.C.C. Henriques, L.M.C. Gato, Experimental compressibility study on a coaxial-duct OWC, in: Proceedings of the 13th European Wave and Tidal Energy Conference, Naples, Italy, 2019.

[46] D.V. Evans, The oscillating water column wave-energy device, J. Appl. Math. 22 (4) (1978) 423–433, http://dx.doi.org/10.1093/imamat/22.4.423.

[47] J. Falnes, Ocean Waves and Oscillating Systems: Linear Interactions Including Wave-Energy Extraction, Cambridge University Press, Cambridge, 2002, http://dx.doi.org/10.1017/CBO9780511754630.

[48] J. Falnes, Wave-energy conversion through relative motion between two single-mode oscillating bodies, J. Offshore Mech. Arct. Eng. 121 (1) (1999) 32–38, http://dx.doi.org/10.1115/1.2829552.

[49] S.L. Dixon, C.A. Hall, Fluid Mechanics and Thermodynamics of Turbomachinery, seventh ed., Butterworth-Heinemann, Oxford, 2013.

[50] E. Dick, Fundamentals of Turbomachines, in: Fluid Mechanics and Its Applications, Springer Netherlands, 2015, http://dx.doi.org/10.1007/978-94-017-9627-9.

[51] J.S. Alves, L.M. Gato, A.F. Falcão, J.C. Henriques, Experimental investigation on performance improvement by mid-plane guide-vanes in a biplane-rotor Wells turbine for wave energy conversion, Renew. Sustain. Energy Rev. 150 (2021) 111497, http://dx.doi.org/10.1016/j.rser.2021.111497.

[52] S.M. Camporeale, P. Filianoti, M. Torresi, Performance of a Wells turbine in an OWC device in comparison to laboratory tests, in: Proceedings of the 9th European Wave and Tidal Energy Conference, Southampton, UK, 2011.

[53] T. Ghisu, P. Puddu, F. Cambuli, Physical explanation of the hysteresis in Wells turbines: A critical reconsideration, J. Fluids Eng. 138 (11) (2016) 111105, http://dx.doi.org/10.1115/1.4033320.

[54] W.K. Tease, J. Lees, A. Hall, Advances in oscillating water column air turbine development, in: Proceedings of the 7th European Wave and Tidal Energy Conference, Porto, Portugal, 2007.

[55] A.A.D. Carrelhas, L.M.C. Gato, J.C.C. Henriques, G.D. Marques, Estimation of generator electrical power output and turbine torque in modelling and field testing of OWC wave energy converters, Energy Conversion and Management: X 19 (2023) 100384, http://dx.doi.org/10.1016/j.ecmx.2023.100384.

[56] A.F.O. Falcão, Control of an oscillating-water-column wave power plant for maximum energy production, Appl. Ocean Res. 24 (2) (2002) 73–82, http://dx.doi.org/10.1016/S0141-1187(02)00021-4.

[57] A.A.D. Carrelhas, L.M.C. Gato, Reliable control of turbine–generator set for oscillating-water-column wave energy converters: Numerical modelling and field data comparison, Energy Convers. Manage. 282 (2023) 116811, http://dx.doi.org/10.1016/j.enconman.2023.116811.

[58] J.C.C. Henriques, A.F.O. Falcão, R.P.F. Gomes, L.M.C. Gato, Air turbine and primary converter matching in spar-buoy oscillating water column wave energy device, in: Proceedings of the 32nd International Conference on Ocean, Offshore and Arctic Engineering, Nantes, France, 2013, http://dx.doi.org/10.1115/OMAE2013-11213.

[59] A.A.D. Carrelhas, L.M.C. Gato, J.C.C. Henriques, A.F.O. Falcão, J. Varandas, Test results of a 30 kW self-rectifying biradial air turbine-generator prototype, Renew. Sustain. Energy Rev. 109 (2019) 187–198, http://dx.doi.org/10.1016/j.rser.2019.04.008.

[60] L.M.C. Gato, A.A.D. Carrelhas, A.F.A. Cunha, Performance improvement of the axial self-rectifying impulse air-turbine for wave energy conversion by multi-row guide vanes: Design and experimental results, Energy Convers. Manage. 243 (2021) 114305, http://dx.doi.org/10.1016/j.enconman.2021.114305.

[61] I.E. Idelchik, M.O. Steinberg, G.R. Malyavskaya, O.G. Martynenko, Handbook of Hydraulic Resistance, Jaico Publishing House, Mumbai, 2008.

[62] T. Sarpkaya, M. Isaacson, Mechanics of Wave Forces on Offshore Structures, Van Nostrand Reinhold Company, New York, 1981.

[63] OpenModelica, OpenModelica: Introduction, 2023, URL https://www.openmodelica.org/. (Accessed 2 March 2023).

[64] Modelica Association, Modelica language, 2023, URL https://www.modelica.org/modelicalanguage. (Accessed 2 March 2023).

[65] M. Otter, D. Winkler, Modelica overview, 2023, URL https://www.modelica.org/education/educational-material/lecture-material/english/ModelicaOverview.pdf. (Accessed 2 March 2023).

[66] R.P.F. Gomes, J.C.C. Henriques, L.M.C. Gato, A.F.O. Falcão, Hydrodynamic optimization of an axisymmetric floating oscillating water column for wave energy conversion, Renew. Energy 44 (2012) 328–339, http://dx.doi.org/10.1016/j.renene.2012.01.105.

[67] J.C.C. Henriques, J.C.C. Portillo, L.M.C. Gato, R.P.F. Gomes, D.N. Ferreira, A.F.O. Falcão, Design of oscillating-water-column wave energy converters with an application to self-powered sensor buoys, Energy 112 (2016) 852–867, http://dx.doi.org/10.1016/j.energy.2016.06.054.

[68] J.C.C. Portillo, Oscillating-water-columns systems: single devices, arrays, and multi-purpose platforms (Ph.D. thesis), Instituto Superior Técnico, University of Lisbon, 2022.

[69] A.J.N.A. Sarmento, Model-test optimization of an OWC wave power plant, Int. J. Offshore Polar Eng. 2 (1993) 66–72.

[70] J. Weber, Optimisation of the hydrodynamic-aerodynamic coupling of an Oscillating Water Column wave energy device (Ph.D. thesis), University College Cork, Ireland, 2006.

[71] F. He, H. Zhang, J. Zhao, S. Zheng, G. Iglesias, Hydrodynamic performance of a pile-supported OWC breakwater: An analytical study, Appl. Ocean Res. 88 (2019) 326–340, http://dx.doi.org/10.1016/j.apor.2019.03.022.

[72] A. LiVecchi, A. Copping, D. Jenne, A. Gorton, R. Preus, G. Gill, R. Robichaud, R. Green, S. Geerlofs, S. Gore, D. Hume, W. McShane, C. Schmaus, H. Spence, Powering the Blue Economy; Exploring Opportunities for Marine Renewable Energy in Maritime Markets, Tech. rep., U.S. Department of Energy, Office of Energy Efficiency and Renewable Energy, Washington, D.C., 2019.

[73] FAO, Global aquaculture production 1950–2018, 2023, URL https://www.fao.org/fishery/en/home. (Accessed 2 March 2023).